

The Rate of Supernovae at Redshift $z \sim 0.1 - 1.0$ – the Stockholm VIMOS Supernova Survey IV [★]

J. Melinder¹, T. Dahlen², L. Mencía Trinchant¹, G. Östlin¹, S. Mattila^{1,3}, J. Sollerman¹, C. Fransson¹, M. Hayes⁴, and S. Nasoudi-Shoar⁵

¹ Department of Astronomy, Oskar Klein Centre, Stockholm University, AlbaNova University Centre, SE-106 91 Stockholm, Sweden
e-mail: jens@astro.su.se

² Space Telescope Science Institute, 3700 San Martin Drive, Baltimore, MD 21218, USA

³ Tuorla Observatory, Department of Physics and Astronomy, University of Turku, Väisäläntie 20, FI-21500 Piikkiö, Finland

⁴ CNRS; Université de Toulouse, UPS-OMP, IRAP, Toulouse, France

⁵ Argelander-Institut für Astronomie, Universität Bonn, Auf dem Hügel 71, 53121 Bonn, Germany

Received ; accepted

ABSTRACT

We present supernova rate measurements at redshift 0.1–1.5 from the Stockholm VIMOS Supernova Survey (SVISS). The sample contains 16 supernovae in total. The discovered supernovae have been classified into core collapse or thermonuclear (Ia) types based on their light curves, colour evolution and host galaxy photometric redshift. The rates we find for the core collapse supernovae are $1.25^{+2.27+0.85}_{-0.97-0.78}$ (with statistical and systematic errors, respectively) at $\langle z \rangle = 0.39$ and $6.90^{+5.24+3.04}_{-3.25-2.14}$ at $\langle z \rangle = 0.73$. For the Ia supernovae the rates are $2.02^{+1.57+0.53}_{-0.96-0.57}$ at $\langle z \rangle = 0.39$ and $1.03^{+0.92+0.31}_{-0.54-0.36}$ at $\langle z \rangle = 0.80$. All of these rate estimates have been corrected for host galaxy extinction. Using Monte Carlo simulations we make a thorough study of the systematic effects from assumptions made when calculating the rates and find that the most important errors comes from misclassification, the assumed mix of faint and bright supernova types and uncertainties in redshift. We compare our rates to other observations, to the star formation history for core collapse rates and to different models of the delay time distribution for Ia rates. Overall, our measurements agree quite well with these other rates when using redshift-dependent corrections for extinction. We do not find any evidence of a missing fraction of core collapse supernovae.

Key words. supernovae – general

1. Introduction

The cosmic rate of supernovae is an important observable that can be used to constrain the properties of galaxies at high redshifts and to study the supernovae themselves. Depending on the origin of the supernova explosion, thermonuclear or core collapse, different subjects can be studied. The first measurement of the cosmic supernova rate was done by Zwicky (1938) who found that “the average frequency of occurrence of supernovae is about one supernovae per extra-galactic nebula per six hundred years” for the local volume. It is not until the latest decades that the higher redshift regimes have been possible to reach.

More recently, large programs targeting Ia supernovae at intermediate and high (> 0.1) redshifts have been conducted to measure the expansion of the universe and do precision cosmology (e.g., Perlmutter et al. 1997; Riess et al. 1998; Astier et al. 2006; Riess et al. 2007). Some of these surveys also report supernova rates for Ia SNe (Neill et al. 2006; Dahlen et al. 2008) out to $z \sim 1.5$ and CC SNe (Dahlen et al. 2004; Bazin et al. 2009) out to $z \sim 0.7$. Large surveys targeting SNe of any type have also been successful in finding and characterising supernovae as well as determining both local and intermediate redshift cosmic supernova rates (Botticella et al. 2008; Dilday et al. 2010; Li et al. 2011b). Sharon et al. (2010) and Dilday et al. (2010) both survey

galaxy clusters, where the SN Ia rates are likely to be enhanced, to find supernovae and have reported cluster SN rates out to redshift 0.9.

The standard observational strategy for finding supernovae at high redshift is to perform a blind survey on a given field and then to monitor the same field as frequently as feasible. The frequency of observations during the survey period are normally chosen to sample signature features of the SN light curves and colour evolution at the target redshifts. In this way photometric typing of the SNe is possible and the light curves can be used to study the SN characteristics. For the Ia surveys with cosmology as the main goal follow-up spectroscopy of SN Ia candidates is needed to get a secure determination of the redshift, confirmation of the type and to improve the accuracy in the distance measurement. When calculating supernova rates from this kind of survey care has to be taken to avoid selection effects from the spectroscopic observations. Supernovae are then detected by searching the images for variable sources, often using image subtraction tools (such as Alard 2000) to minimise subtraction residuals.

Supernova typing normally includes studying the spectra of the SNe close to peak and identifying spectral lines, notably H, He and SiII lines, something which is observationally very expensive and in practice unfeasible at high redshift for fainter SN types. Another method to type SNe is to compare the observed light curves and colour evolution to pre-existing templates of different SN types, i.e. photometric SN typing. These methods have been demonstrated to work (e.g., Kuznetsova & Connolly

[★] Based on observations collected at the European Organisation for Astronomical Research in the Southern Hemisphere, Chile, under ESO programme ID 167.D-0492.

2007; Poznanski et al. 2007; Rodney & Tonry 2009; Kessler et al. 2010) using somewhat different techniques. Better typing accuracy is achieved with prior information on the redshift through photometric or spectroscopic redshift of the host galaxy (Melinder et al. 2011; Kessler et al. 2010).

Thermonuclear supernovae (or Ia SNe) are white dwarfs that explode when they accrete matter and approach the Chandrasekhar limit (see Leibundgut 2000, for a review). When taking the luminosity-stretch relation (Phillips et al. 1999) into account the peak luminosity of these SNe exhibit a very narrow spread and can thus be used to measure cosmological distances (see references above). The exact details of the explosions and the progenitor system are not fully understood. For example, the time between formation of the progenitor system and the supernova explosion – the so called delay time – is unknown. This delay time depends on the nature of the companion star to the white dwarf (Greggio 2005). By studying the rates of Ia supernovae and comparing to either the cosmic star formation history (e.g. Neill et al. 2006; Strolger et al. 2010), or the star formation rates and stellar masses of the host galaxies (Sullivan et al. 2006; Totani et al. 2008; Maoz et al. 2011) it is possible to set constraints on the delay time and thereby also on the progenitor system.

Core collapse supernova explosions (CC SNe) are the end-points of the lives of massive stars, with masses between $\sim 8M_{\odot}$ and $\sim 50M_{\odot}$ (Nomoto 1984; Tsujimoto et al. 1997; Smartt 2009). Since massive stars are short-lived compared to the cosmic timescales the supernovae trace active star formation. By averaging the CC SN rate over cosmic volume the current star formation in that volume can be studied. In this way an independent measure of the star formation history at high redshift can be obtained (Dahlen et al. 2004; Cappellaro et al. 2005; Botticella et al. 2008; Bazin et al. 2009). More conventional methods of finding the cosmic star formation rates include measuring the rest-frame UV light from galaxies at a given redshift (as in, e.g., Giavalisco et al. 2004; Bouwens et al. 2009), measuring the FIR light to take star formation hidden by dust into account (e.g. Le Floch et al. 2005) and deriving the rates from $H\alpha$ measurements (Shim et al. 2009; Hayes et al. 2010). The UV and $H\alpha$ -based methods have a drawback, that is also present for the supernova rate method, in that a correction for dust extinction need to be applied. Methods based on using the far-IR light to estimate the added star formation from re-radiated UV light make it possible to correct the star formation history for dust extinction effects. Hopkins & Beacom (2006) presented a compilation of the star formation history from multiple sources for $z \sim 0 - 6$, taking the obscured star formation into account, and fitted an analytical function to the data.

The light from a supernova has to pass through its host galaxy before starting on the long trip to reach our telescopes. When travelling through the gas and dust inside its host the supernova light will be subject to varying degrees of extinction, depending on the dust content of the galaxy and the position of the SNe with respect to the observer (e.g., light from a supernova situated in an edge-on galaxy will suffer from high extinction). Hatano et al. (1998) and Riello & Patat (2005) present models of extinction for core collapse and thermonuclear SNe in normal spiral galaxies. These models are built by using Monte Carlo simulations of supernova positions within a galaxy with given morphology and dust content. By using the extinction models it is possible to estimate the effect on the the observed supernova rates (Dahlen et al. 2004). It should be noted that this method is only valid for normal galaxies with low to medium amounts of gas/dust, typical of galaxies in the local volume of the universe.

As we go to higher and higher redshifts, more and more of the star formation takes place inside dusty galaxies. Le Floch et al. (2005) find that the star formation from these infrared bright objects dominate the global star formation at redshift 0.7 and higher. In these galaxies much of the light from an exploding supernova is absorbed on its way out. For low to moderate amounts of extinction this can be estimated and taken into account in the light curve analysis. But for host galaxies with high dust content (such as luminous and ultra-luminous infrared galaxies, LIRGs and ULIRGs) most of the supernovae might not even be detectable, even in near-IR where the extinction is strongly reduced (e.g., Mattila & Meikle 2001). When calculating the rates, the number of missing SNe due to the change in average extinction in star forming galaxies with redshift needs to be compensated for (Mannucci et al. 2007).

The Stockholm VIMOS Supernova Survey (SVISS) is a multi-band ($R+I$) imaging survey aiming to detect supernovae at redshift ~ 0.5 and derive thermonuclear and core-collapse supernova rates. The supernova survey data were obtained over a six month period with VIMOS/VLT (LeFevre et al. 2003). Melinder et al. (2008) describe the supernova search method along with extensive testing of the image subtraction, supernova detection and photometry. The discovery and typing of 16 supernovae in one of the search field is reported in Melinder et al. (2011, submitted). In this paper we present the supernova rates estimated from the survey data along with delay time distributions for the Ia SNe and star formation rates calculated from the CC SNe rates.

The first part of the paper contains a description of the observations and supernova sample. In Section 3 we describe the method used to determine the supernova rates and in Section 4 the resulting supernova rates, delay time distribution and star formation rates are presented. In the final section of the paper, Section 5, we discuss the results and compare them to the work of other authors. The Vega magnitude system and a standard Λ CDM cosmology with $\{h_0, \Omega_M, \Omega_{\Lambda}\} = \{70, 0.3, 0.7\}$ have been used throughout the paper.

2. The Data

2.1. Observations

The data were obtained with the VIMOS instrument (LeFevre et al. 2003) mounted on the ESO Very Large Telescope (UT3) at several epochs during 2003–2006. The VIMOS instrument has four CCDs, each $2k \times 2.4k$ pixels with a pixel scale of $0.205''/\text{pxl}$, covering a total area of roughly 4×56 sq. arcmin. The observations were obtained in the ELAIS-S1 field (La Franca et al. 2004), in five broad band filters (U, B, V, R and I) centred at $\alpha = 00 : 32 : 13, \delta = -44 : 36 : 27$ (J2000). The supernova search filters are R and I . Observations in these filters have been divided into seven search epochs and 2 additional reference epochs (one before and one after). The search epochs are separated by roughly one month.

The individual frames in each epoch were reduced, including removal of fringes, registered to a common frame of reference and stacked. Each epoch image was photometrically calibrated using spectrophotometric standard stars observed during one of the nights and tertiary standard stars selected in the field. Detailed measurements of the seeing in each of the frames were done by modelling the point spread function using the IRAF psf task.

2.2. The Supernova Sample

The supernovae were detected by using a dedicated pipeline that was developed and thoroughly tested by our team. For a detailed description along with the results of the testing please consult Melinder et al. (2008). The pipeline includes the following steps, first the reference image and the search image are scaled to a common seeing by using the ISIS 2.2 code (Alard 2000) and the reference image subtracted from the search image. Automatic source detection using SExtractor (Bertin & Arnouts 1996) together with a by-eye inspection is then done on the subtracted image to find variable objects. The final step in the pipeline is the acquisition of photometry, aperture and PSF modelling based, also in the subtracted frame. Detailed simulations of the photometric accuracy is also done to make sure that the error estimates are valid. To avoid including spurious detections in the output catalogues we require that the supernova candidates are detected in both bands in two consecutive epochs. A detection is here defined as being brighter than the 3σ limiting magnitude in that epoch. Furthermore, we used the late control epoch to remove non-SNe (most likely AGN) from the sample, since no SNe are expected to be visible ~ 1 year after explosion at the wavelengths and redshifts considered here.

For the sample of supernovae considered in this paper we used the pipeline described above on the ELAIS-S1 $R + I$ data and found a total of 16 supernovae, eight thermonuclear (Ia-like) and eight core collapse supernovae ranging from $z \sim 0.1$ to $z \sim 1.5$ (see Table 1). The light curves and colour evolution of the SNe were used to classify them into either Ia-like or core collapse types. We then co-added the likelihoods for each main type (Ia and CC) to find the most likely type. This was done using a Bayesian model selection code, where priors were used for the redshift (host galaxy photometric redshift), absolute magnitude distribution, extinction and time after explosion. In Melinder et al. (2011, submitted) we describe how the sample was obtained in detail together with the typing code used to find the types. In this paper we also investigated the misclassification errors when applying our code to the SN sample by using a Monte Carlo simulated sample of ~ 18000 SNe and a local SN sample from SDSS-II containing 87 SNe. The resulting errors are given as misclassification ratios, f_{loss} , f_{gain} where, e.g., $f_{loss}(TN)$ refers to the percentage of thermonuclear SNe that are mistyped as core

Table 1. Supernovae in the SVISS

SVISS ID	Type	Subtype	P(Type)	z
SVISS-SN43	Ia	Ia-normal	0.888	0.43
SVISS-SN161	Ia	Ia-faint	1.00	0.50
SVISS-SN115	Ia	Ia-91t	1.00	0.40
SVISS-SN116	Ia	Ia-faint	1.00	0.55
SVISS-SN309	Ia	Ia-faint	1.00	0.47
SVISS-SN402	Ia	Ia-faint	1.00	0.22
SVISS-SN135	Ia	Ia-normal	0.978	0.98
SVISS-SN14	Ia	Ia-normal	0.716	0.66
SVISS-SN51	CC	IIP	1.00	0.52
SVISS-SN54	CC	IIn	0.863	0.84
SVISS-SN261	CC	Ibc-bright	0.574	0.78
SVISS-SN55	CC	IIP	0.987	0.82
SVISS-SN31	CC	IIL	0.999	0.12
SVISS-SN56	CC	Ibc-bright	0.920	0.57
SVISS-SN357	CC	IIn	1.00	1.49
SVISS-SN24	CC	Ibc-bright	0.511	0.82

Notes. P(Type) is the probability (Bayesian evidence) for the best fitting main type (TN/CC).

Table 2. Misclassification percentages

z	f_{gain}	f_{loss}	dz
Thermonuclear Supernovae			
$z \leq 0.5$	0.071	0.022	0.11
$0.5 < z \leq 1.0$	0.067	0.031	0.081
$1.0 < z \leq 1.5$	0.052	0.0078	0.094
Core-collapse Supernovae			
$z \leq 0.5$	0.015	0.049	0.10
$0.5 < z \leq 1.0$	0.042	0.091	0.087
$1.0 < z \leq 1.5$	0.0035	0.023	0.14

Notes. f_{gain}/f_{loss} are the misclassification ratios (see text) and dz is the redshift variance (based on the fitted redshift from the typing code compared to the true redshift of the supernova) for the specific bin.

collapse SNe. These ratios are given in Table 2 for different redshift bins and types.

2.3. Supernova Redshifts

The reference epoch R and I images were used together with the UBV deep images to obtain photometric redshifts for the supernova host galaxies. The redshifts are calculated by using the GOODSZ code (Dahlen et al. 2010). This is a χ^2 template fitting code that uses empirical spectral energy distributions from Coleman et al. (1980) and Kinney et al. (1996). Details on the photometric redshift technique will be presented in Mencía Trinchant (in prep.). We require the galaxies to be detected in at least 3 filters to trust the resulting redshifts, something which is fulfilled for all of the 16 supernovae. The hosts were selected by choosing the closest galaxy in physical distance, calculating the distance by using the photometric redshift and the angular distance. For two of the supernovae (SN309 and SN357) this means that the closest galaxy in terms of angular distance is not the host galaxy. These galaxies are at a lot higher redshifts ($z \gtrsim 3$), thus we would not even be able to detect a supernovae in them. More details on the host galaxy identification will be presented

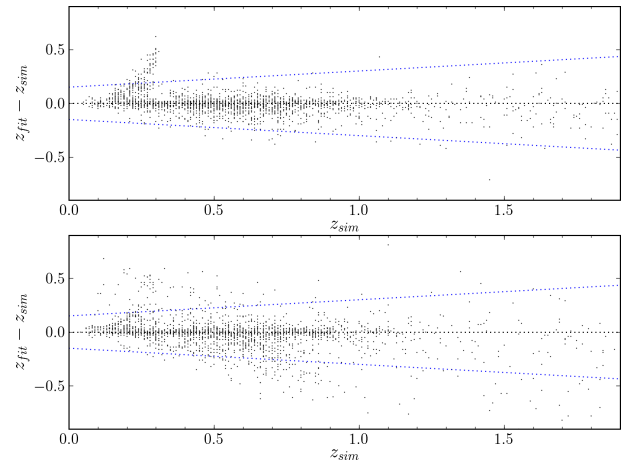


Fig. 1. The figure shows the resulting redshift accuracy for supernovae with (upper panel) and without (lower panel) a host galaxy photometric redshift. The ~ 2000 SNe of all different subtypes used to make this figure are a sub-sample of the full sample of simulated light curves. The redshift on the x axis (z_{sim}) is the initial adopted redshift of the supernovae. The (red) dotted lines indicate the $|z_{fit} - z_{sim}| / (1 + z_{sim}) > 0.15$ limits. (This figure is available in colour in the electronic version of the article)

in Melinder et al. (2011, submitted) and Mencía Trinchant et al. (in prep.).

The photometric redshifts, together with the 68% confidence limits (as estimated by the χ^2 fitting), were used to construct a Bayesian prior for the supernova typing. The typing code then outputs a most likely redshift for the best fitting supernova type for each supernova (details will be given in Melinder et al., 2011, submitted). This is the redshift estimate used for the supernovae in the rate calculations. Figure 1 shows the redshift accuracy for the Monte Carlo simulated supernova sample described in Section 2.2. The host galaxy photometric redshifts were assumed to have an accuracy of $\delta z = 0.07$ where the redshift scatter Δz is given by $\Delta z = \delta z(1 + z)$. The resulting redshift accuracy for the SNe with host galaxy redshifts is given by $\delta z = 0.07$ with an outlier fraction (defined as having having $|z_{sim} - z_{fit}| > 0.15$) of 3% over the full range of redshifts. For reference, we also show the accuracy for SNe typed with a flat redshift prior (i.e. sources without any photometric redshift information). This is worse, with $\delta z = 0.11$ and an outlier fraction of 4%. For both populations it should be noted that the major part of the outliers comes from the $z_{sim} = 0.2 - 0.4$ region and is due to mistyping of the supernovae.

The typing was also rerun using a flat redshift prior for all of the discovered SNe. The fitted redshifts from this run were all within the 68% confidence limit of the host photometric redshifts and none of the SNe changed main type. Based on this the chosen hosts are thus likely to be the correct ones, although it is certainly possible that some hosts have been misidentified. In any case, neither the typing nor redshifts are appreciably affected by the possible host misidentification.

3. Supernova Rate Determination

The supernova rates were determined by using a Monte Carlo method (Dahlen et al. 2004). Using a set of supernova templates (see Table 3) we simulate a number of supernova light curves of different types and at different redshifts with time of explosion set within our observational window (approximately 5 months before until 5 months after the monitoring). The main input parameters are the intrinsic supernova rates (Ia and CC) for a given redshift bin and volume-limited fractions of the different types. The template light curves are calculated from absolute magnitude light curves (mainly from Richardson et al. 2002; Dahlen et al. 2004; Richardson et al. 2006) and a set of spectra from Nugent (2007). For more information on how the template light

curves are built see Melinder et al. (2011, submitted) and references therein.

The volumetric fractions for the Ia subtypes are adapted from Li et al. (2011b), treating their Ia-HV sub category as Ia-normal SNe. The Ia-faint category is used in the typing of supernovae to be able to better characterise normal Ia supernovae with a somewhat lower value of stretch. The fraction of low-stretch Ia SNe is estimated from the distribution of stretch value in the SNLS (Sullivan et al. 2006) Ia sample. The core collapse fractions are based on a compilation of supernovae from Smartt et al. (2009) and Li et al. (2011b), treating IIb SNe as Ibc-normal supernovae, with our time sampling of the light curves these subtypes will look very similar.

Each supernova is also given a host galaxy extinction. For Type Ia SNe we use the parameterisation of the Riello & Patat (2005) simulations presented in Neill et al. (2006). The work of Riello & Patat (2005) was done primarily for Ia supernovae, for core collapse SNe we therefore instead use simulations by Erkki Kankare (2011, in prep) that are based on the models of Hatano et al. (1998). To calculate the wave-length dependence of the extinction, we use a Cardelli extinction law (Cardelli et al. 1989) with $R_V = 3.1$ for Type Ia SNe and a Calzetti extinction law (Calzetti et al. 2000) with $R_V = 4.05$ for core collapse SNe. In Section 4.3, we investigate how the choice of extinction models and extinction laws affects the results.

The light curves are then fed through the same detection procedure as the real supernova light curves (see Section 2.2). It should be noted that even with a quite conservative photometric limit (3σ in four data points) there are issue with completeness. The detection efficiency of the survey does affect the observed rates since it starts to drop below one before the 3σ -limit is reached. The detection efficiencies described below are thus used to give a probability that a supernova is detected in a certain epoch and filter, and are included in the Monte Carlo simulations. We have used the detection efficiencies derived for hosts of intermediate brightness for all supernovae. The effect of this choice on the rates is small (see Section 4.3).

The output number of detectable SNe from the simulations are then compared to the observed number in the chosen redshift bins. Since the redshifts for the SNe have quite high uncertainties (being based on photometric redshifts) we distribute the SNe in the bins according a Gaussian distribution with the redshift uncertainty ($0.07(1 + z)$). The simulations are rerun until the output number match the observed number. At that point the input intrinsic SN rate that produces the correct number of observed SNe is chosen as the true supernova rate.

Table 3. Properties of the supernova photometric templates

Type	$\langle M_B \rangle$	σ_M	Fraction	
Ia – 91T	-19.64	0.30	1.04	0.10
Ia – normal	-19.34	0.50	1.00	0.52
Ia – faint	-18.96	0.50	0.80	0.18
Ia – 91bg	-17.84	0.50	0.49	0.20
Ibc – bright	-19.34	0.46	N/A	0.0160
Ibc – normal	-17.03	0.49	N/A	0.327
IIIL	-17.23	0.38	N/A	0.055
IIIn	-18.82	0.92	N/A	0.055
IIP	-16.66	1.12	N/A	0.547

Notes. $\langle M_B \rangle$ is the absolute magnitude in the Johnson-B filter at peak (assuming standard Λ CDM cosmology $\{h_0, \Omega_M, \Omega_\Lambda\} = \{70, 0.3, 0.7\}$), σ_M is the dispersion in the peak magnitude. Fraction refers to the fraction within each main type in a volume limited sample.

3.1. Detection Efficiencies

The detection efficiency for each epoch and filter was determined by simulating supernovae at variable brightness in the actual search images and then running the standard detection pipeline on the simulated frames. The procedures used are described in Melinder et al. (2008). We placed supernovae in different environments, i.e. with different host galaxy brightness, to study the effect of background light on the efficiencies. The detection efficiencies are notably worse when the SNe are situated in bright galaxies (defined as having $m_I > 22$). In Figure 2 a sample of the detection efficiency testing is presented, showing the efficiencies for the three different host galaxy brightness modes. It should be noted that the 50% efficiency limits roughly corresponds to the 3σ rejection limits.

To use the efficiency curves in the Monte Carlo simulations, and to smooth out possible outliers in the measured efficiency,

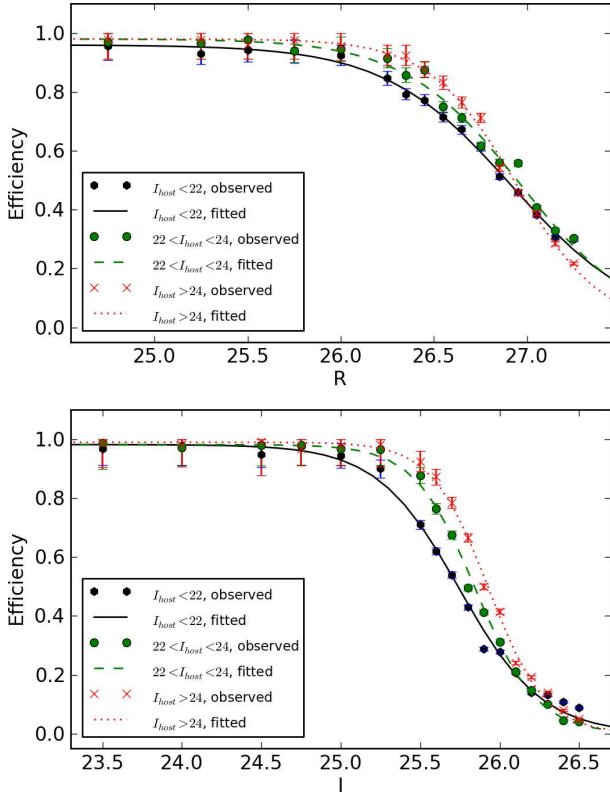


Fig. 2. This figure shows an example of the detection efficiency for a given epoch for different host galaxy brightness. The efficiencies from simulations of supernovae in the field are given by the point markers while the lines are the s-curve fits to the efficiencies as described in the text. Errors for the measure efficiencies are binomial. Note that a total of 30 (one for each of 5 epochs \times 2 filters \times 3 host galaxy types) s-curve fits have been used to estimate the detection efficiencies of the full survey. (This figure is available in colour in the electronic version of the article)

we parametrise the efficiencies using a S-curve parametrisation (as previously used by, e.g., Strolger et al. 2004) given by:

$$\epsilon(m) = \frac{\epsilon_0}{1 + e^{(m-m_c)/S}}, \quad (1)$$

where $\epsilon(m)$ is the fitted detection efficiency and m the magnitude. ϵ_0 is the maximum efficiency (which is very close to 1 for most of our fits), m_c a parameter describing when the curve starts to drop of and S a parameter that determines how fast the drop occurs. The best-fitting parameters for each epoch, filter and host galaxy brightness are found with a simple χ^2 optimisation algorithm and are shown as lines in Figure 2

3.2. Correcting the Rates for Dust Obscuration in LIRGs/ULIRGs

Supernovae in the local universe are mostly discovered in galaxies with low amounts of dust. This is not surprising, given that the extinction will cause SNe to be fainter and thus harder to detect. The global star formation in the local universe takes place mostly in galaxies with low extinction. The use of core collapse supernovae as tracers of recent star formation is thus feasible at low redshifts. But as we go to higher redshifts the bulk of star formation is no longer taking place in these low-extinction galaxies but rather in galaxies with large amounts of dust (in LIRGs and ULIRGs). Le Flocc'h et al. (2005) find that approximately 70 % of the star formation at $z \sim 1$ is taking place in

LIRGs, and present how this fraction changes with redshift from low to high redshift. From now on we denote this effect *obscuration*, to distinguish it from the normal host galaxy extinction for spiral and elliptical galaxies discussed in Section 3.

Mannucci et al. (2007) have used these results together with their estimate[S] on how many SNe are lost due to obscuration by dust in local galaxies to derive a correction for supernova rates at high redshifts. This correction is given by the function:

$$f_{CC}(z) = 0.05 + 0.28z, \quad (2)$$

valid for $z \leq 2$ and where f_{CC} is the fraction of supernovae missed at redshift z . We apply this correction to our core collapse supernova rates (Table 4 contains rates with and without this correction).

Ia SNe are not as strongly coupled to star formation as core collapse SNe. There are some indications that there are two channels for Ia supernovae to explode, one prompt (and therefore coupled to the star formation) and one delayed (). The prompt component will be obscured to the same extent as the CC SNe while the delayed component is far less susceptible to this effect. However, some of these Ia SNe will still go off in dusty galaxies and a correction (albeit smaller) should be applied also for them. Taking both channels into account, Mannucci et al. (2007) find a correction factor of:

$$f_{Ia} = 0.02 + 0.12z^{1.4}, \quad (3)$$

valid for $z \leq 2$ for the Ia rates. It should be noted that this correction is more uncertain than the one for CC given in Equation 2, given that it depends critically on the assumed DTD. This correction is applied to the SVISS Ia rates.

4. Results

4.1. Core Collapse Supernova Rates

The core collapse supernova rate in two redshift bins (0.1–0.5, 0.5–0.9) is shown in Figure 3 and in Table 4. We also show the rates when including SVISS-SN357, the $z = 1.49$ core collapse SNe in our sample, with different redshift binning (0.1–0.8, 0.8–1.5). We do not exclude this SNe because the typing and redshift in themselves are in doubt, but rather that having such large redshift bins cause the errors of the rate estimate to become very large. We therefore consider the rates calculated using the smaller redshift bins to be the main determination in this paper. Both the rates corrected for extinction/obscuration and the raw rates are shown in the table but the figure show the corrected values. The errors shown in the figure are statistical only (systematic errors are given in the table), unless otherwise noted.

The figure also shows a comparison of our rates with rates reported by other authors. At low redshift we plot the rate estimates of LOSS (Li et al. 2011a), which is the largest SN survey to date in the local volume with a total number of core collapse SNe of 440. We also plot the low redshift rate determined by Cappellaro et al. (1999). At slightly higher redshifts we plot the results from Cappellaro et al. (2005) and Botticella et al. (2008). The second survey with rates based on a large number of CC SNe (117 SNe) is the Supernova Legacy Survey (SNLS, Bazin et al. 2009) which provides a data point with low error at $z = 0.3$. At higher redshifts we plot the rates from the GOODS determined by Dahlen et al. (2004) and the recent measurements from the Subaru Deep Field (Graur et al. 2011). The lines in the figure are estimates of the star formation history from two different sources, Strolger et al. (2004) and Hopkins & Beacom (2006),

Table 4. Supernova rates

z	$\langle z \rangle$	$R_{Ia/CC} \times 10^{-4}$ (with ext. cor.)	$R_{Ia/CC} \times 10^{-4}$ (no ext. cor.)	N_{raw}	N_{redist}
Ia Supernovae					
$z < 0.5$	0.39	$2.02^{+1.57+0.53}_{-0.96-0.57}$	$1.69^{+1.31+0.44}_{-0.81-0.47}$	4	4.12
$0.5 \geq z < 1.0$	0.80	$1.03^{+0.92+0.31}_{-0.54-0.36}$	$0.71^{+0.21+0.21}_{-0.37-0.25}$	4	3.43
CC Supernovae					
$0.1 < z < 0.5$	0.39	$1.25^{+2.27+0.85}_{-0.97-0.78}$	$0.781^{+1.41+0.53}_{-0.60-0.48}$	1	1.36
$0.5 \geq z < 0.9$	0.73	$6.90^{+5.24+3.04}_{-3.25-2.14}$	$2.89^{+2.19+1.27}_{-1.35-0.90}$	6	4.27
$0.1 \geq z < 0.8$	0.57	$2.81^{+2.09+1.74}_{-1.30-1.74}$	$1.48^{+1.09+0.92}_{-0.68-0.92}$	4	4.44
$0.8 \geq z < 1.5$	1.18	$10.1^{+10.6+4.44}_{-5.82-3.13}$	$3.60^{+4.08+1.58}_{-2.08-1.12}$	4	2.73

Notes. $\langle z \rangle$ is the volume averaged redshift over the given redshift range. The supernova rates $R_{Ia/CC}$ are in units of $\text{yr}^{-1} \text{Mpc}^{-3} h_{70}^3$ and given with and without corrections for extinction and obscuration. N_{raw} is the raw number of supernovae per bin and N_{redist} is the number when taking the redshift uncertainty into account.

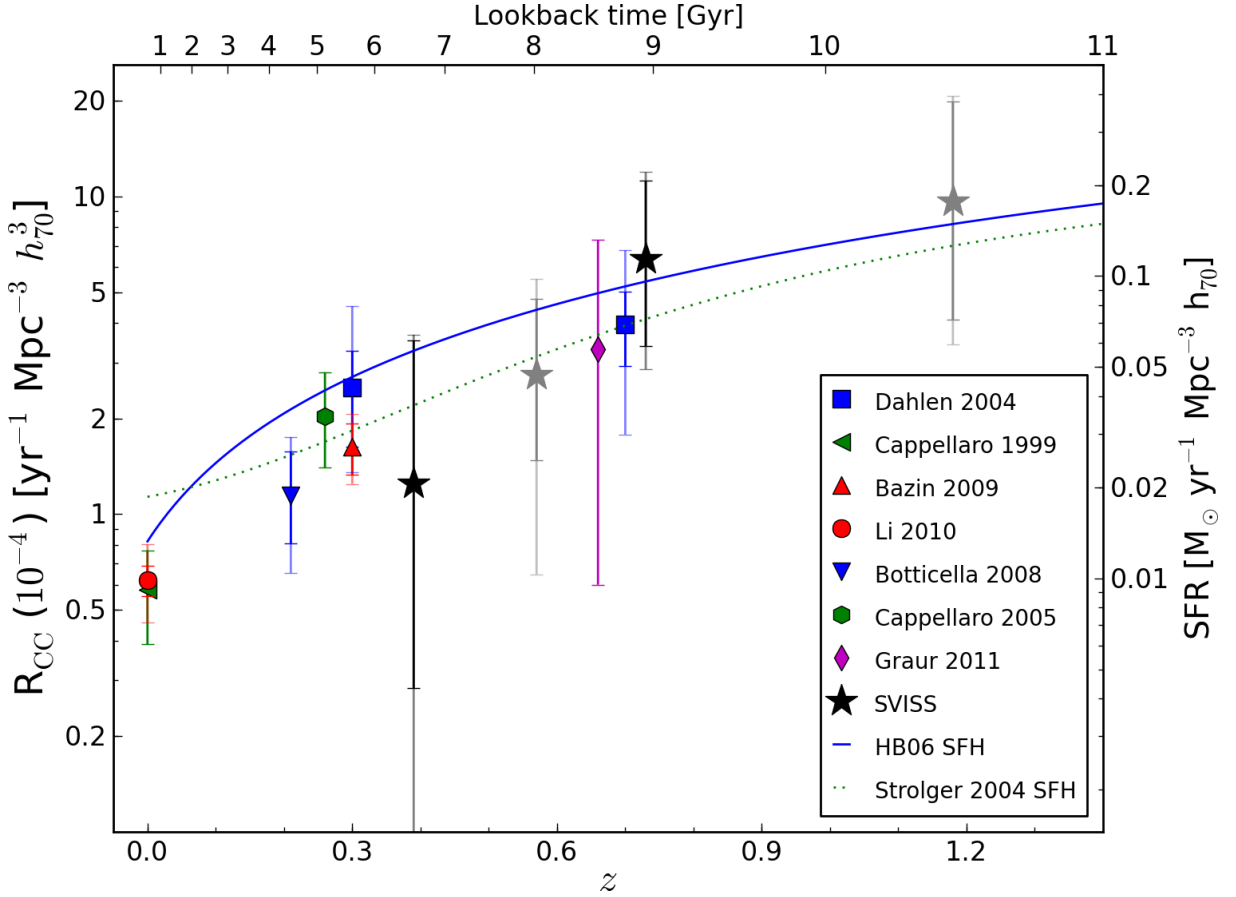


Fig. 3. Core collapse supernova rates determined from the SVISS SNe (black stars, grey stars for different binning) together with a collection of measured rates from other authors (see legend for symbols and references). We also plot star formation histories from two different sources, scaled to supernova rates through the use of Equation 4. Error bars are statistical with total errors (statistical and systematic added in quadrature) as a transparent/faded extra error bar for all surveys. Redshift bin sizes are not shown, but are given in Table 4. The rate from Cappellaro et al. (1999) has been rescaled from SNU to a volumetric rate by assuming a local B-band luminosity density $2.0 \times 10^8 h L_{sun} \text{Mpc}^{-3}$ at redshift ~ 0 . (This figure is available in colour in the electronic version of the article)

scaled to supernova rates (see Section 4.4). Both are corrected for extinction.

The rate at $z = 0.39$ is fairly low but consistent with the rates reported by other authors. Our CC rate at high redshift agree well with the observations of Dahlen et al. (2004) and Graur et al. (2011). For a discussion on how our supernova rate measurements compares to the star formation history see Section 5.

4.2. Ia Supernova Rates

The Ia supernova rate in two redshift bins ($0-0.5, 0.5-1.0$) is shown in Figure 4 and in Table 4. The rates in the table are given with and without extinction/obscuration correction.

At low z we show the Ia rates from the LOSS (Li et al. 2011a) and Cappellaro et al. (1999). At slightly higher z we compare with the rates calculated from the SDSS supernova

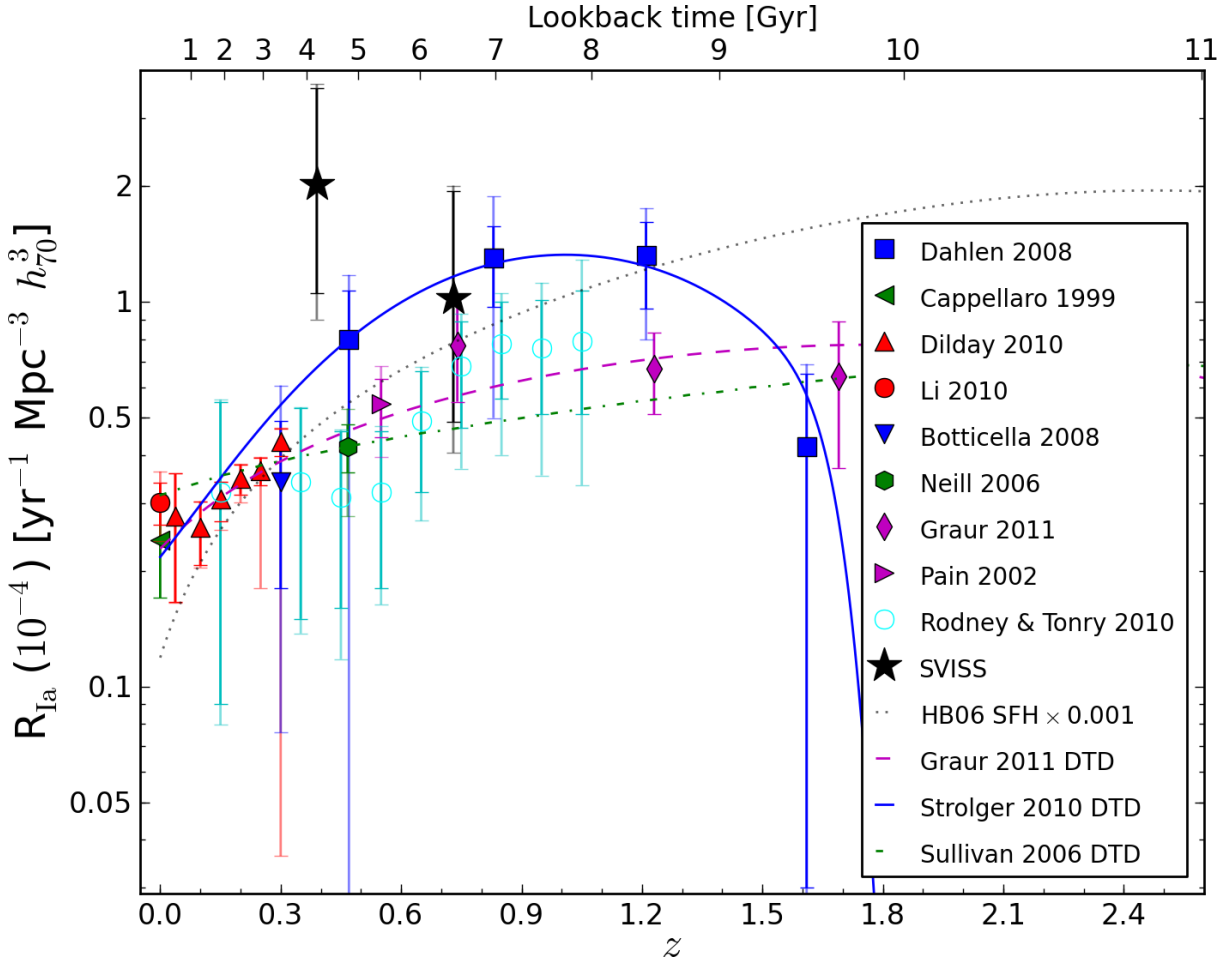


Fig. 4. Ia supernova rates determined from the SVISS SNe (black stars) together with a collection of measured rates from other authors (see legend for symbols and references). We also plot Ia rates resulting from assumptions on the delay time distribution combined with the star formation history. Error bars are statistical with total errors (statistical and systematic added in quadrature) as a transparent/faded extra error bar for all surveys. Redshift bin sizes are not shown, but are given in Table 4. The rate from Cappellaro et al. (1999) has been rescaled from SNU to a volumetric rate by assuming a local B-band luminosity density $2.0 \times 10^8 h_{70}^3 \text{ Mpc}^{-3}$ at redshift ~ 0 . (This figure is available in colour in the electronic version of the article)

search (Dilday et al. 2010) and with the results from the STRESS (Botticella et al. 2008). Rodney & Tonry (2010) present revised Ia rates from the IfA Deep Survey out to $z = 1.05$ using new techniques, lower than those previously reported. The SNLS measures the Ia rate at $z = 0.47$ using a large sample of supernovae, at similar redshift Pain et al. (2002) presented some of the first rates determined from cosmological survey data. At higher redshifts Dahlen et al. (2008) determined Ia rates from the GOODS (extending their sample from 2004). Recently Graur et al. (2011) reported the findings of the supernova search in the Subaru Deep Field, their rate measurements are (together with the GOODS results) the highest redshift measurements available and reach $z \sim 1.7$.

The low redshift rate measurement is significantly higher than the results from other surveys. We think that this is due to a combination of small number statistics and systematic errors in the shape of mistyping and discuss it further in Section 5. While the accuracy of our rate measurements are too low (and at too low redshifts) to make any detailed fitting of different DTD models, we still compare our rates to models introduced by other authors (Sullivan et al. 2006; Neill et al. 2006; Strolger et al. 2010; Graur et al. 2011) together with their chosen star formation history (see Section 4.5 for details).

4.3. Analysis of Errors for the Supernova Rates

The statistical errors are calculated using the prescription of Gehrels (1986). The redshift bins have been chosen to provide a reasonable number of sources in each bin to get similar statistical errors in each bin.

We now proceed to study the systematic errors of our rate estimates. Since the total number of SNe are quite low, the statistical errors are high. The main goal of this study is thus to find out whether any of the systematic effects can introduce errors larger than these. Calculating the mean statistical relative error (mean of the upper and lower limit differences) for the two types and all redshift bins we arrive at the following: 129% for CC, low z ; 61% for CC, high z ; 63% for Ia, low z ; and 71% for Ia, high z . These can be compared to the relative systematic errors calculated below. A compilation of the systematic errors can be found in Table 5.

Misclassification errors The systematic errors due to misclassification in our sample can be found in Table 2 and are on the order of 5–10%. However, these estimates are really only valid when the number of detected SNe is large enough. For the small number statistic estimates presented here the systematic errors

Table 5. Systematic errors

Error	CC Supernovae		Ia Supernovae	
	$0.1 < z < 0.5$	$0.5 < z < 0.9$	$0 < z < 0.5$	$0.5 < z < 1.0$
Misclassification	51%	17%	22%	22%
Redshift	32%	16%	15%	20%
Detection eff.	2%	3%	1%	2%
Photometric	4%	9%	2%	5%
Template choices	+31%	+32%	+1/-8%%	+2%/-17%
Peak magnitudes	7%	15%	2%	3%
Extinction laws	$\lesssim 1\%$	10%	2%	2%
Total systematic	+68/-62%	+44/-31%	+26/-28%	+30/-35%
Statistical	129%	61%	63%	71%

Notes. Errors are two-sided unless the sign is given.

have to be estimated in a different way. The expected numbers of misclassified SNe in each type and redshift bin is below one in all cases. To get a conservative estimate of the misclassification systematic error we thus vary the observed number of SNe by one (positive and negative) and recalculate the rates. This test gives an error of approximately 20%, but is dependent on the actual number of sources in the given bin (a low source count gives a higher error). For bins with more than 2 supernovae the error is smaller than the statistical errors.

The systematic misclassification errors are overestimated when computed with this method, on average one SNe in our sample will have been misclassified, not one per bin and type as the estimate indicates. But it is impossible to say which bin and type that is affected by misclassification, hence we give this error estimate.

Redshift The redshifts of the supernovae have uncertainties on the order of 0.1 when using the host photometric redshifts as a prior for the typing. This leads to a redistribution in redshift which affects the rates. To study this effect we redistribute the simulated SNe according to a Gaussian distribution assuming $\sigma = 0.07(1+z)$ and recalculate the rates. This test is repeated 10,000 times to find the spread in the rates. The systematic error varies between ~ 15 to $\sim 30\%$ for the different types and redshift bins, lower than the statistical errors in all cases.

Detection efficiencies We determine the systematic errors from the detection efficiency assumptions by using the faint and bright host galaxy detection efficiency estimates. The binomial errors of the efficiencies are smaller than the difference between the results for the different host types in almost all cases. The effect on the rates is on the order of $\pm 2\%$, significantly lower than the statistical errors.

Photometric errors The SVISS photometric zeropoint calibration is accurate to within $\sim 5\%$. Since we apply an absolute 3σ detection limit on our sample (see Section 2.2) the estimated rates will be affected by a slight shift in the photometric zeropoints. This effect will of course in reality be random over the two filters and seven epochs, to get a conservative estimate we vary the detection limits by 0.1 magnitude. The resulting rates vary by $\sim 5\%$.

Template choices Our selection of subtype light curve templates and their assumed fractions influence the rates as well. The choices and assumptions we have made are based on obser-

vational results (Richardson et al. 2002, 2006; Li et al. 2011b). The fractions are subject to statistical uncertainties as well as systematic uncertainties (e.g. evolution with redshift, selective obscuration). There is also the possibility that very faint supernovae are underrepresented in magnitude-limited SN surveys (Horiuchi et al. 2011).

For the CC SNe we study the effect of introducing an additional light curve template, a IIP template with a peak M_B of -14.39 (as for the faint core collapse SN 1987A) with fraction that changes the percentage of CC SNe with $M_B < -15$ from 7% to 30%. The effect of this change on the rates is quite large, it makes the rates go up by approximately 30%. This is smaller than the statistical errors but could possibly help explain any possible mismatch with the star formation history (as identified by Horiuchi et al. 2011). Varying the fractions randomly have a very small effect on the rates since the changes tend to cancel out.

For the Ia SNe we have made tests with different combinations of using or not using the peculiar (91t and 91bg-like) and non-standard (Ia-faint) templates. We get the largest positive change in the rates when putting the fraction of 91t SNe to zero (treating them as normal Ia SNe), on the order of 1–2%. The largest negative change is found when setting the fraction of faint Ia supernovae (91bg and the Ia-faint subtypes) to zero, treating them as Ia-normal SNe, which results in a change of 10–15% in the rates. These errors should be considered to be the extreme limits, since there is plenty of evidence that these faint Ia SNe do exist.

Peak magnitudes As described above the choice of template distribution also affects the distribution of peak magnitudes for the simulated SNe. However, the average peak magnitudes used in this work have associated uncertainties (note that this is not the same as the scatter).

For the CC SNe the template peak magnitudes have uncertainties given by Richardson et al. (2002) and Richardson et al. (2006). As conservative estimate we allow the peak magnitudes of CC SNe to vary by the 1σ errors given in these papers and recompute the rates. The resulting rates change by approximately 10%, which is smaller than the statistical errors.

For the Ia SNe the peak magnitudes are much better constrained (due to their use in precision cosmology). Assuming an uncertainty of 0.05 magnitudes for the Ia subtype and 0.1 for the 91bg/91t subtypes we calculate the impact on the Ia rates. The effect is small, on the order of 3%, much smaller than the statistical errors.

Host galaxy extinction The assumptions on extinction and obscuration in the host galaxies will also affect the rates. The obscuration corrections for higher redshifts given by Mannucci et al. (2007) do not have any associated uncertainties. Furthermore, these estimates are based on a small number of SNe detected in local LIRGs. More work is therefore needed to put proper confidence limits on these corrections. We thus choose to give rate values both with and without any corrections for dust obscuration, but do not calculate any associated systematic errors due to the assumptions on obscuration corrections.

The effect of host galaxy extinctions are based on models by Riello & Patat (2005) and Hatano et al. (1998) for Type Ia and core collapse SNe, respectively. Using instead a positive Gaussian distribution of $E(B-V)$ with $\sigma E(B-V)=0.2$ as in Neill et al. (2006) for Type Ia only changes the rate by $\sim 2\%$. For core collapse SNe, we have also examined the effect of applying an extinction model following Riello & Patat (2005). This has marginal effect on the rate in the low redshift bin ($< 1\%$) and may affect the high redshift bin by 10% .

The effect of host galaxy extinctions as estimated by Riello & Patat (2005) have been used for both SN types. Using the estimates from Hatano et al. (1998) change the resulting rates by a very small amount ($< 1\%$). We also study the effect of using different extinction laws for the extinction. For the CC SNe we use a Cardelli/ $R_V = 3.1$ law instead of the Calzetti law and for the Ia we use a steeper Cardelli law with $R_V = 2.1$ (as advocated by Goobar 2008). The impact on the rates is small, on the order of 1% .

AGN contamination We used a control epoch with observations obtained one year after our search period had ended to check whether any of our supernova candidates showed variability over this longer period. Except for the possibility of very rare peculiar SNe none of the SN subtypes would be detected one year later. The list of variable sources originally contained 31 entries, about 10 of which showed variability over along timescale and were excluded from the final list of SNe. This routine is enough to limit the amount of AGN contamination to very low levels. We do not give this error in Table 5 since we estimate it to be smaller than all other systematic effects.

In Table 5 we also give the sum of all the systematic errors (added in quadrature). These are also the systematic error estimates given in Table 4. The co-added systematic errors are roughly half of the statistical errors. It should be noted that this estimate is very conservative, the systematic errors we have studied are not independent errors and some effects will very likely cancel out. The main contribution to the systematic errors come from misclassification, followed by template choices for the CC SNe and redshift uncertainties for both types.

4.4. Comparing the CC Supernovae Rate to the Cosmic Star Formation History

The core collapse supernova rate can be compared to the cosmic star formation history, since the timescale for CC progenitors to explode is much shorter than the cosmic timescale. The supernova rate is derived from the star formation history by assuming an Initial Mass Function (IMF, denoted by ξ below) and the mass range of the SN progenitors (M_l and M_u for the lower and upper mass limits, respectively). The volumetric rate of CC SNe, R_{CC} in units of $\text{yr}^{-1} \text{Mpc}^{-3}$ is then:

$$R_{CC}(z) = k \times \rho_*(z), \quad (4)$$

where $\rho_*(z)$ is the star formation history in units of $\text{M}_\odot \text{yr}^{-1} \text{Mpc}^{-3}$. R_{CC} is a volumetric rate, and thus scales as h^3 , this needs to be addressed when comparing to star formation histories which may have a different scaling. The constant k is the percentage of stars that explode as SNe per unit mass and is given by:

$$k = \frac{\int_{M_l}^{M_u} \xi(M) dM}{\int_{0.1\text{M}_\odot}^{125\text{M}_\odot} M \xi(M) dM}. \quad (5)$$

For this work we choose to use a Salpeter IMF (Salpeter 1955) with progenitor masses between 8M_\odot and 50M_\odot . The constant k is then equal to 0.0069.

The choice to use a Salpeter IMF is based on that most SFH measurements and other supernova rate measurements are using this IMF. Recently a number of authors have argued that the Salpeter IMF is not consistent with recent observations (see, e.g., Hopkins & Beacom 2006), and claim that an IMF with a flatter shape is better. The choice to use different IMFs introduce a systematic uncertainty to the comparison. However, the IMF dependence is partly cancelled out by the dependence on IMF of the star formation history (where the IMF is used to normalise the star formation measurements). To investigate this we compute k for the flattest IMF given in Hopkins & Beacom (2006) which is a modified Salpeter form from Baldry & Glazebrook (2003) with a high mass slope of -1.15 (compared to -1.35 for the normal Salpeter IMF). While the k factor changes by to 0.0141 (changing by a factor 2.03) this is countered by the change of the SFH normalisation by a factor of 0.50, given by Hopkins & Beacom (2006). The total change of the SNR–SFR comparison is thus on the order of 2% , significantly less than the statistical errors. Incidentally, this also tells us that there is little hope in trying to use the comparisons between SNR and star formation rates to constrain a possible universal IMF unless a lot larger supernova samples can be obtained.

The upper limit for the progenitor mass comes from Tsujimoto et al. (1997) and is essentially the limit at which massive stars will become black holes instead of neutron stars with an associated supernova explosion. Varying the upper limit between $M_u = [30, 125] \text{M}_\odot$ has a small effect on the SNR–SFR comparison, less than 10% , although this could be slightly higher with a flatter IMF. The lower limit of 8M_\odot is grounded on observations of supernova progenitors (Smartt et al. 2009). The choice of lower limit affect the rate scaling strongly but is luckily well constrained by these observations, varying the lower limit between their 68% confidence limits ($7-9.5 \text{M}_\odot$) changes k by $\pm 20\%$, also this lower than the statistical errors for our supernova rates.

4.4.1. Star formation history parametrisations

We use star formation histories ($\rho_*(z)$) from two different sources as input for Equation 4. Hopkins & Beacom (2006) compile star formation measurements from many sources and correct them for dust extinction based on the work done by Le Floch et al. (2005). The observations are then fit by the simple analytical parametrisation introduced by Cole et al. (2001):

$$\rho_*(z) = \frac{(a + bz)h}{1 + (z/c)^d}, \quad (6)$$

where a , b , c and d are fitting parameters and h is the Hubble constant to account for changes to the assumed cosmology. The best fit from Hopkins & Beacom (2006) give parameter values:

$a = 0.0170$, $b = 0.13$, $c = 3.3$ and $d = 5.3$. They give a conservative error estimate by plotting the confidence regions of the fit, at $z \sim 1$ the uncertainty is on the order of 30%.

Strolger et al. (2004) fit the data compilation of Giavalisco et al. (2004) by using a parametrisation of the form:

$$\rho_*(t) = a(t^b e^{-t/c} + d e^{d(t-t_0)/c}), \quad (7)$$

where a , b , c and d are parameters, t is the age of the universe and t_0 the age of the universe at $z = 0$ (13.47 Gyrs with our chosen cosmology). The best fit parameter values are: $a = 0.182$, $b = 1.26$, $c = 1.865$ and $d = 0.071$. To compare this with our results we convert it to $\rho_*(z)$.

4.5. Delay Time Distributions for Ia Supernovae

The delay time distribution (DTD) for Ia supernovae is an interesting subject and is the subject of controversy in current research. By convolving an assumed DTD with the underlying star formation history the Ia rate can be calculated. This can then be compared with the observed rates to put constraints on the DTDs. The Ia rate can thus be written (Strolger et al. 2004):

$$R_{Ia}(t) = \nu \int_{t_0}^t \rho_*(t') \Phi(t-t') dt', \quad (8)$$

where ν is the number of SNe formed per unit stellar mass, $\rho_{*}(t)$ the star formation history and $\Phi(\tau)$ the delay time distribution which represents the percentage of supernovae that go off at time τ after a single burst of star formation. Also, t_0 is the time at which stars start to form in the universe, we assume this happens at $z = 10$; corresponding to a time of 0.45 Gyrs after the big bang (with our chosen cosmology). The integral can easily be converted to redshift space to yield $R_{Ia}(z)$ by performing a variable substitution.

As noted above, the uncertainties in our rate estimates make it quite fruitless to try and fit different DTDs to our data. Instead we choose to compare our rates to the best-fitting DTDs from other authors. In Figure 4 we show four different choices of DTD. The simplest one is just a rescaling of the star formation history assuming that one Ia SNe explode per $1000M_{\odot}$ of stellar mass formed (Neill et al. 2006). This corresponds to using a Dirac delta function DTD with the peak at $\tau = 0$, i.e., no delay time between the SN explosion and star formation or, in other words, a prompt channel for the Ia progenitor-to-supernova process.

In Strolger et al. (2010) and Strolger et al. (2004) a Gaussian shaped (or close to Gaussian) DTD with a mean delay time of ~ 3 Gyrs is found to give the best fit to the GOODS Ia supernova rates. We use the unimodal skew-normal DTD parametrisation and best fitting parameters from Strolger et al. (2010) and convolve this with the star formation history given in Equation 7 (the same SFH as the one used by these authors). The DTD parametrisation is:

$$\Phi(\tau) = \frac{1}{\omega\pi} e^{-\frac{(\tau-\xi)^2}{2\omega^2}} \int_{-\text{inf}}^{\alpha(\frac{\tau-\xi}{\omega})} e^{-t'^2/2} dt', \quad (9)$$

with the best fitting parameters $\omega = 0.2$, $\xi = 3.2$ and $\alpha = 2.2$.

Graur et al. (2011) fit the results from the SDF supernova search together with the rates of many other surveys using different power law DTDs. The DTD models and SFHs they try show quite similar fitting quality, the rate we show in Figure 4 uses a power law DTD with an exponent β equal to 0.97, their best fitting value:

$$\Phi(\tau) = \Phi_1 \tau^{\beta}, \quad (10)$$

where Φ_1 is a normalisation parameter. Φ is also set to 0 for $\tau < 40$ million years. This is then convolved with the SFH given in Equation 6 from Hopkins & Beacom (2006) to get the rates plotted in the figure.

Scannapieco & Bildsten (2005), Mannucci et al. (2006) and Sullivan et al. (2006) find strong evidence for the existence of a prompt channel for Ia SNe by looking at the properties of the host galaxies of Ia SNe (and other data). Maoz et al. (2011) study the hosts of the local SNe found in the LOSS and find a prompt channel (with $\tau < 420$ Myrs) with 99% significance. Models of Ia explosions also show the possibility of such a channel (Nomoto et al. 2009; Ruiter et al. 2010). The Ia rates are then modelled with one prompt component, directly proportional to the SFH, and one delayed component. We plot the resulting Ia rate from the work by Sullivan et al. (2006), who use a parametrisation of the form

$$R_{Ia}(t) = A \int_0^t \rho_*(t') dt' + B \rho_*(t). \quad (11)$$

Note that the SFH used by us is not strictly the same as the one used by these authors and can thus not be used directly in this equation. We plot the SNR as given in Sullivan et al. (2006) in Figure 4.

5. Discussion and Summary

We have presented supernova rates from the SVISS along with a description of the methods used to compute them and an extensive analysis of systematic errors for the rates. The resulting rates for the core collapse SNe are: $1.25^{+2.27+0.85}_{-0.97-0.78}$ (with statistical and systematic errors, respectively) at $\langle z \rangle = 0.39$, $6.90^{+5.24+3.04}_{-3.25-2.14}$ at $\langle z \rangle = 0.73$; or, $2.81^{+2.09+1.74}_{-1.30-1.74}$ at $\langle z \rangle = 0.57$ and $10.1^{+10.6+4.44}_{-5.82-3.13}$ at $\langle z \rangle = 1.15$ with a different redshift binning. These rates have been corrected for high redshift obscuration by using the prescription of Mannucci et al. (2007) and host galaxy extinction (Riello & Patat 2005). Un-corrected values can be found in Table 4.

Our rate estimates follows the star formation history well, within the statistical errors, although the low- z bin is marginally low. Due to the somewhat suspiciously high value of the Ia rate in the same z bin, and the misclassification testing that indicates that approximately one ($8\% \sim 7\%$) Ia supernova should be misclassified over the $z = 0 - 1$ range, it is very possible that the low z CC rate should be higher. If we assume that one of the low z Ia SNe is misclassified the $\langle z \rangle = 0.39$ rate increases to 1.65 (this is indicated by a slightly offset arrow in the Figure 3).

Horiuchi et al. (2011) point out that the core collapse supernova rates found in both local and high redshift searches seem to be too low by a factor of two when compared to the star formation history compiled in Hopkins & Beacom (2006). Our results do not show this difference, both of our rate estimates are consistent with the star formation history within the statistical errors. But our errors are of course quite high, the rates estimated by other authors, in particular at low z , does in fact differ significantly from the SFH. The strongest evidence for this comes from the rate estimate by Li et al. (2011a) at low z which has small errors and is clearly below the SFH. At higher redshift the problem is less severe, which could be due to the increased statistical errors. At high redshift the problem may also be somewhat alleviated by the obscuration corrections, which we have included in our plotted rates in Figure 3, the rates from other surveys plotted in this figure do not include this correction (with the exception of the data point from Graur et al. 2011).

Horiuchi et al. (2011) suggest that taking missed SNe due to extinction and dust obscuration in LIRGs and ULIRGs into account is not enough to explain the difference. Instead they suggest that the reason is that the assumed fractions of faint and very faint CC SNe are too low. In our tests of the systematic uncertainties we find that assuming 30% of the CC SNe to be faint ($M_B < -15$) boost the rates by $\sim 30\%$, not enough to bridge the factor of two gap found for the local SN searches. Of course, the assumption on fractions of faint CC SNE may be very different for the different surveys, making it possible that other data points may go up more than this. Thus larger correction factors for extinction and dust obscuration in LIRGs and ULIRGs can still be needed to explain the difference between the predicted and observed CC SN rates both locally and at higher z . While the SFHs we compare with have also been corrected for dust and hidden star formation, the supernovae are probably affected differently by the presence of obscuring dust. The number of supernovae that are missed in dusty starburst galaxies and LIRGs is currently not well constrained even in the local universe (Mannucci et al. 2003; Kankare et al. 2008; Mattila et al. 2004).

High angular resolution observations at near-IR (e.g., Mattila et al. 2007; Kankare et al. 2008) and radio (e.g. Pérez-Torres et al. 2010; Romero-Canizales et al. 2011) wavelengths have recently been used to detect and characterise the hidden SN populations in the nearest LIRGs. Such studies are needed to constrain the complete rates, properties and extinction distributions towards the CC SNe buried in such dusty galaxies. Eventually, these studies will provide a robust estimate for the numbers of SNe missed by optical searches both locally and at high- z .

The resulting rates for the Ia supernovae are: $2.02_{-0.96}^{+1.57+0.53}$ at $\langle z \rangle = 0.39$ and $1.03_{-0.54}^{+0.92+0.31}$ at $\langle z \rangle = 0.80$. Also these rates have been corrected for high redshift obscuration and host galaxy extinction.

As mentioned above, the high Ia rate obtained for the low z bin could be due to one of the SNe in this bin being misclassified as a Ia SNe. If we assume that one of the SNe in this bin is misclassified the Ia rate at $\langle z \rangle = 0.39$ changes to 1.56 (again indicated in Figure 4 by an arrow), which makes this rate measurement consistent with other rates and models.

Due to the quite high statistical errors and the lack of Ia SNe beyond $z = 1$ we do not try to fit any DTDs to our Ia rate measurements. The comparison to the plotted models show (looking at the high- z data point) show that all the plotted models but the two-component one from Sullivan et al. (2006) are consistent with our rates. The two-component model is still perfectly acceptable though, given that our rates are subject to additional systematic errors not shown in the figure. Strolger et al. (2010) find that models with a prompt Ia component are hard to reconcile with the rates measured at redshifts higher than one, increased sample sizes at these high redshifts, or more studies of Ia host galaxies (Gallagher et al. 2005; Sullivan et al. 2006) are needed to constrain the contribution from this channel.

The determination of supernova rates at high redshift is sensitive to a number of assumptions made during the calculations. To estimate the systematic errors these assumptions give rise to is important. With the exception of the misclassification error, that essentially scales with the sample size for samples smaller than 10 given a misclassification ratio of 10%, we have shown that the systematic errors are on the order of 50% when using photometric redshifts and with the present uncertainties in template fractions and peak magnitudes. Furthermore, the assumptions made when correcting the rates for extinction/obscuration are also subject to systematics. Presently little is known about

the number of SNe missed in LIRGs and ULIRGs, which is especially important at high redshift.

Given the low numbers of SNe for most high redshift surveys it is perhaps tempting to try and use the rates found in different surveys together when comparing to models (for the Ia SNe) and other sources (SFH for CC SNe). It's not straight-forward to do this, however. Different surveys study different systematic errors, some include more sources and some less. If combined as given using co-added statistical and systematic errors, the risk is that greater weight is given to surveys where fewer systematic error estimates are included (given that the sample sizes are similar). We believe that the work presented in this paper shows the importance of including a variety of systematic effects to correctly estimate the uncertainties of supernova rates at high redshift. This will be even more important for future surveys with larger sample sizes and therefore lower statistical errors.

Acknowledgements. We are grateful for financial support from the Swedish Research Council. S.M. and J.M. acknowledge financial support from the Academy of Finland (project:8120503).

References

- Alard, C. 2000, *A&AS*, 144, 363, (A00)
- Astier, P., Guy, J., Regnault, N., et al. 2006, *A&A*, 447, 31
- Baldry, I. K. & Glazebrook, K. 2003, *ApJ*, 593, 258
- Bazin, G., Palanque-Delabrouille, N., Rich, J., et al. 2009, *A&A*, 499, 635
- Bertin, E. & Arnouts, S. 1996, *A&AS*, 117, 393
- Botticella, M. T., Riello, M., Cappellaro, E., et al. 2008, *A&A*, 479, 49
- Bouwens, R. J., Illingworth, G. D., Franx, M., et al. 2009, *ApJ*, 705, 936
- Calzetti, D., Armus, L., Bohlin, R. C., et al. 2000, *ApJ*, 533, 682
- Cappellaro, E., Evans, R., & Turatto, M. 1999, *A&A*, 351, 459
- Cappellaro, E., Riello, M., Altavilla, G., et al. 2005, *A&A*, 430, 83
- Cardelli, J. A., Clayton, G. C., & Mathis, J. S. 1989, *ApJ*, 345, 245
- Cole, S., Norberg, P., Baugh, C. M., et al. 2001, *MNRAS*, 326, 255
- Coleman, G. D., Wu, C., & Weedman, D. W. 1980, *ApJS*, 43, 393
- Dahlen, T., Mobasher, B., Dickinson, M., et al. 2010, *ApJ*, 724, 425
- Dahlen, T., Strolger, L.-G., & Riess, A. G. 2008, *ApJ*, 681, 462
- Dahlen, T., Strolger, L.-G., Riess, A. G., et al. 2004, *ApJ*, 613, 189
- Dilday, B., Smith, M., Bassett, B., et al. 2010, *ApJ*, 713, 1026
- Gallagher, J. S., Garnavich, P. M., Berlind, P., et al. 2005, *ApJ*, 634, 210
- Gehrels, N. 1986, *ApJ*, 303, 336
- Giavalisco, M., Dickinson, M., Ferguson, H. C., et al. 2004, *ApJ*, 600, L103
- Goobar, A. 2008, *ApJ*, 686, L103
- Graur, O., Poznanski, D., Maoz, D., et al. 2011, *ArXiv e-prints*
- Greggio, L. 2005, *A&A*, 441, 1055
- Hatano, K., Branch, D., & Deaton, J. 1998, *ApJ*, 502, 177
- Hayes, M., Schaerer, D., & Östlin, G. 2010, *A&A*, 509, L5+
- Hopkins, A. M. & Beacom, J. F. 2006, *ApJ*, 651, 142
- Horiuchi, S., Beacom, J. F., Kochanek, C. S., et al. 2011, *ArXiv e-prints*
- Kankare, E., Mattila, S., Ryder, S., et al. 2008, *ApJ*, 689, L97
- Kessler, R., Bassett, B., Belov, P., et al. 2010, *PASP*, 122, 1415
- Kinney, A. L., Calzetti, D., Bohlin, R. C., et al. 1996, *ApJ*, 467, 38
- Kuznetsova, N. V. & Connolly, B. M. 2007, *ApJ*, 659, 530
- La Franca, F., Gruppioni, C., Matute, I., et al. 2004, *AJ*, 127, 3075
- Le Floc'h, E., Papovich, C., Dole, H., et al. 2005, *ApJ*, 632, 169
- LeFevre, O., Saisse, M., Mancini, D., et al. 2003, in *Presented at the Society of Photo-Optical Instrumentation Engineers (SPIE) Conference, Vol. 4841, Instrument Design and Performance for Optical/Infrared Ground-based Telescopes*. Edited by Iye, Masanori; Moorwood, Alan F. M. *Proceedings of the SPIE, Volume 4841*, pp. 1670-1681 (2003), ed. M. Iye & A. F. M. Moorwood, 1670-1681
- Leibundgut, B. 2000, *A&A Rev.*, 10, 179
- Li, W., Chornock, R., Leaman, J., et al. 2011a, *MNRAS*, 317
- Li, W., Leaman, J., Chornock, R., et al. 2011b, *MNRAS*, 413
- Mannucci, F., Della Valle, M., & Panagia, N. 2006, *MNRAS*, 370, 773
- Mannucci, F., Della Valle, M., & Panagia, N. 2007, *MNRAS*, 377, 1229
- Mannucci, F., Maiolino, R., Cresci, G., et al. 2003, *A&A*, 401, 519
- Maoz, D., Mannucci, F., Li, W., et al. 2011, *MNRAS*, 307
- Mattila, S. & Meikle, W. P. S. 2001, *MNRAS*, 324, 325
- Mattila, S., Meikle, W. P. S., & Greimel, R. 2004, *New Astronomy Review*, 48, 595
- Mattila, S., Väisänen, P., Farrah, D., et al. 2007, *ApJ*, 659, L9

- Melinder, J., Mattila, S., Östlin, G., Mencia Trinchant, L., & Fransson, C. 2008, *A&A*, 490, 419
- Neill, J. D., Sullivan, M., Balam, D., et al. 2006, *AJ*, 132, 1126
- Nomoto, K. 1984, *ApJ*, 277, 791
- Nomoto, K., Kamiya, Y., Nakasato, N., Hachisu, I., & Kato, M. 2009, in *American Institute of Physics Conference Series*, Vol. 1111, American Institute of Physics Conference Series, ed. G. Giobbi, A. Tornambe, G. Raimondo, M. Limongi, L. A. Antonelli, N. Menci, & E. Brocato, 267–276
- Nugent, P. 2007, Peter Nugent’s Spectral Templates, http://supernova.lbl.gov/~nugent/nugent_templates.html
- Pain, R., Fabbro, S., Sullivan, M., et al. 2002, *ApJ*, 577, 120
- Pérez-Torres, M. A., Alberdi, A., Romero-Cañizales, C., & Bondi, M. 2010, *A&A*, 519, L5+
- Perlmutter, S., Gabi, S., Goldhaber, G., et al. 1997, *ApJ*, 483, 565
- Phillips, M. M., Lira, P., Suntzeff, N. B., et al. 1999, *AJ*, 118, 1766
- Poznanski, D., Maoz, D., & Gal-Yam, A. 2007, *AJ*, 134, 1285
- Richardson, D., Branch, D., & Baron, E. 2006, *AJ*, 131, 2233
- Richardson, D., Branch, D., Casebeer, D., et al. 2002, *AJ*, 123, 745
- Riello, M. & Patat, F. 2005, *MNRAS*, 362, 671
- Riess, A. G., Filippenko, A. V., Challis, P., et al. 1998, *AJ*, 116, 1009
- Riess, A. G., Strolger, L., Casertano, S., et al. 2007, *ApJ*, 659, 98
- Rodney, S. A. & Tonry, J. L. 2009, *ApJ*, 707, 1064
- Rodney, S. A. & Tonry, J. L. 2010, *ApJ*, 723, 47
- Romero-Canizales, C., Mattila, S., Alberdi, A., et al. 2011, *ArXiv e-prints*
- Ruiter, A. J., Belczynski, K., Sim, S. A., et al. 2010, *ArXiv e-prints*
- Salpeter, E. E. 1955, *ApJ*, 121, 161
- Scannapieco, E. & Bildsten, L. 2005, *ApJ*, 629, L85
- Sharon, K., Gal-Yam, A., Maoz, D., et al. 2010, *ApJ*, 718, 876
- Shim, H., Colbert, J., Teplitz, H., et al. 2009, *ApJ*, 696, 785
- Smartt, S. J. 2009, *ARA&A*, 47, 63
- Smartt, S. J., Eldridge, J. J., Crockett, R. M., & Maund, J. R. 2009, *MNRAS*, 395, 1409
- Strolger, L., Dahlen, T., & Riess, A. G. 2010, *ApJ*, 713, 32
- Strolger, L., Riess, A. G., Dahlen, T., et al. 2004, *ApJ*, 613, 200
- Sullivan, M., Le Borgne, D., Pritchett, C. J., et al. 2006, *ApJ*, 648, 868
- Totani, T., Morokuma, T., Oda, T., Doi, M., & Yasuda, N. 2008, *PASJ*, 60, 1327
- Tsujimoto, T., Yoshii, Y., Nomoto, K., et al. 1997, *ApJ*, 483, 228
- Zwicky, F. 1938, *ApJ*, 88, 529